A Broadband and Scalable Model for On-Chip Inductors Incorporating Substrate and Conductor Loss Effects

Jyh-Chyurn Guo and Teng-Yang Tan

***Abstract*—A new T-model has been developed to accurately simulate the broadband characteristics of on-Si-chip spiral inductors, up to 20 GHz. The spiral coil and substrate *RLC* networks built in the model play a key role responsible for conductor loss and substrate loss in the wideband regime, which cannot be accurately described by the conventional π-model. Good match with the measured *S*-parameters, $L(\omega)$, $\mathrm{Re}(Z_{\mathrm{in}}(\omega))$, and $Q(\omega)$ proves the proposed T-model. Besides the broadband feature, scalability has been justified by good match with a linear function of coil numbers for all model parameters employed in the *RLC* networks. The satisfactory scalability manifest themselves physical parameters rather than curve fitting. A parameter extraction flow is established through equivalent circuit analysis to enable automatic parameter extraction and optimization. This scalable inductor model will facilitate optimization design of on-chip inductor and the accuracy proven up to 20 GHz can improve RF circuit simulation accuracy demanded by broadband design.**

***Index Terms*—Broadband, inductor, lossy substrate, scalable.**

I. Introduction

THE LACK of an accurate and scalable model for on-chip inductors becomes one of the most challenging problems for Si-based RF integrated circuit (IC) design. The existing models suffer two major drawbacks in terms of accuracy for limited bandwidth and poor scalability. Many publications reported improvement on the commonly adopted π-model by modification on the equivalent circuit scheme [1]–[3]. However, limited bandwidth to few gigahertz remains an issue for most of the modified π-models. A two-π model was proposed to improve the accuracy of $R(\omega)$ and $L(\omega)$ beyond self-resonance frequency [4]. Unfortunately, this two-π model suffers a singular point above resonance [5]. Besides, the complicated circuit topology with double element number will lead to difficulty in parameter extraction and greater time consumption in circuit simulation [6]. Recent work using modified T-model demonstrated promising improvement in broadband accuracy and suggested the advantage of T-model over π-model [7]. However, the scalability of model's major concern was not reported. In our paper, a T-model of new circuit scheme is proposed to realize two primary features, i.e., broadband accuracy and scalability. Our T-model is composed of two *RLC* networks to account for spiral coils, lossy substrate, and their mutual interaction. Four physical elements, R_S, L_S, R_P, and C_P are incorporated to describe the spiral coils above Si substrate and other four elements, R_{sub}, C_{sub}, L_{sub} and R_{loss} are employed to account for the lossy substrate. C_{ox} allocated between two RLC networks is responsible for coupling between two networks, i.e., the spiral inductor and lossy substrate. All the physical elements are constants independent of frequencies and can be expressed by a close form derived from circuit analysis on the proposed T-model. Parameter extraction and optimization can be conducted with an initial guess extracted by approximation valid for specified frequency range. All the model parameters manifest themselves with predictable scalability w.r.t. coil numbers and physical nature. A parameter extraction flow has been established to enable automatic parameter extraction and optimization that is easy to be adopted by existing circuit simulators like Agilent ADS or parameter extractor such as Agilent IC-Cap. The model accuracy over broadband is validated by good agreement with the measured *S*-parameters, $L(\omega)$, $\mathrm{Re}(Z_{\mathrm{in}}(\omega))$, and $Q(\omega)$ up to 20 GHz ($\mathrm{Re}(Z_{\mathrm{in}})$ is the real part of input impedance). It is expected that this scalable inductor model can effectively improve RF circuit simulation accuracy in broad bandwidth and facilitate the design optimization using on-chip inductors.

Manuscript received September 8, 2005; revised December 2, 2005. This work was supported in part by the National Science Council of Taiwan, R.O.C. under Grant 93-2220-E009-018 and Grant 94-2220-E009-018.

The authors are with the Department of Electronics Engineering, National Chiao-Tung University, Hsinchu 300, Taiwan, R.O.C. (e-mail: jcguo@mail.nctu.edu.tw).

Digital Object Identifier 10.1109/TED.2005.864409

II. Technology and Characterization

Spiral inductors of square coils were fabricated by 0.13 μm back end technology with eight layers of Cu and low-*k* intermetal dielectric $\mathrm{k} = 3.0$). The top metal of 3 μm Cu was used to implement the spiral coils of width fixed at 15 μm and intercoil space at 2 μm. The inner radius is 60 μm and outer radius is determined by different coil numbers$N = 2.5$, 3.5, 4.5, and 5.5 for this paper. The physical inductance achieved at sufficiently low frequency are around 1.96$\sim$8.66 nH corresponding to coil numbers $N = 2.5 \sim 5.5$. *S*-parameters were measured by using Agilent network analyzer up to 20 GHz and de-embedding was carefully done to extract the truly intrinsic characteristics for model parameter extraction and scalable model build up.

III. T-Model's Equivalent Circuit and Model Parameter Extraction Flow

A. T-Model Equivalent Circuit Schematics and Analysis

Fig. 1(a) illustrates the circuit schematics of the proposed T-model for on-chip inductors in which two *RLC* networks of four physical elements for each part are linked through C_{ox} to

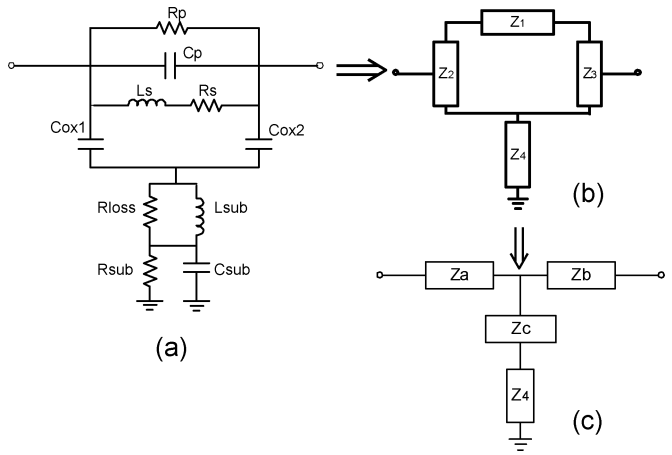

Fig. 1. T-model for on-chip spiral inductors. (a) Equivalent circuit schematics. (b) Intermediate stage of schematic block diagrams for circuit analysis. (c) Final stage of schematic block diagrams for circuit analysis.

account for the coupling between the spiral inductors and lossy substrate underneath. The physical property is defined for each element in the equivalent circuit. R_S and L_S represent the spiral metal coil's series resistance and inductance respectively. R_P is a new parameter created in our model to account for spiral coil's conductor loss originated from lossy substrate return path. C_P indicates the inter-coil and under-pass capacitance and $C_{\rm ox}$ accounts for the spiral coil to substrate coupling capacitance. $R_{\rm sub}$ and $C_{\rm sub}$ represent the lossy substrate resistance and capacitance. $L_{\rm sub}$ and $R_{\rm loss}$ are two more new elements created in our model to describe the eddy current induced substrate loss. $L_{\rm sub}$ accounts for the reactive power loss crossing the substrate and $R_{\rm loss}$ is responsible for the resistive loss or joule heat dissipation. Fig. 1(b) indicates the schematic block diagrams derived by circuit analysis theory to extract the physical circuit elements as proposed. Z_1 represents the *RLC* network for spiral inductor and Z_4 is another one representing lossy substrate. $Z_2 = Z_3 = 1/(\mathrm{j}\omega C_{\rm ox})$ acts as the coupling path between Z_1 and Z_4. The circuit scheme is further transformed to Fig. 1(c) to correlate with *Y*-parameters from 2-port measurement.

B. Model Parameter Extraction and Optimization Principle

All the unknown *R, L, C* parameters are extracted from analytical equations derived from equivalent circuit analysis as shown in Fig. 1. The analytical equations are composed of *Z*- and/or *Y*-parameters listed in the first block of extraction flow illustrated in Fig. 2, which can be easily transformed from the measured *S*-parameter after appropriate de-embedding. Under the condition that the number of unknown elements is larger than the number of equations (for most of complicated problems like this one), the approximation valid under very low or very high frequency is generally made to remove some unknown elements and extract the remaining ones as the first step, and then to extract the others at the second step. Due to the necessary approximation, the extracted *R,L,C* parameters in the first run of flow (Fig. 2) are generally not the exactly correct solutions but just serve as the initial guess for further optimization through best fitting to the measured *S*-parameters, $L(\omega)$, $\mathrm{Re}(Z_{\rm in}(\omega))$, and $Q(\omega)$.

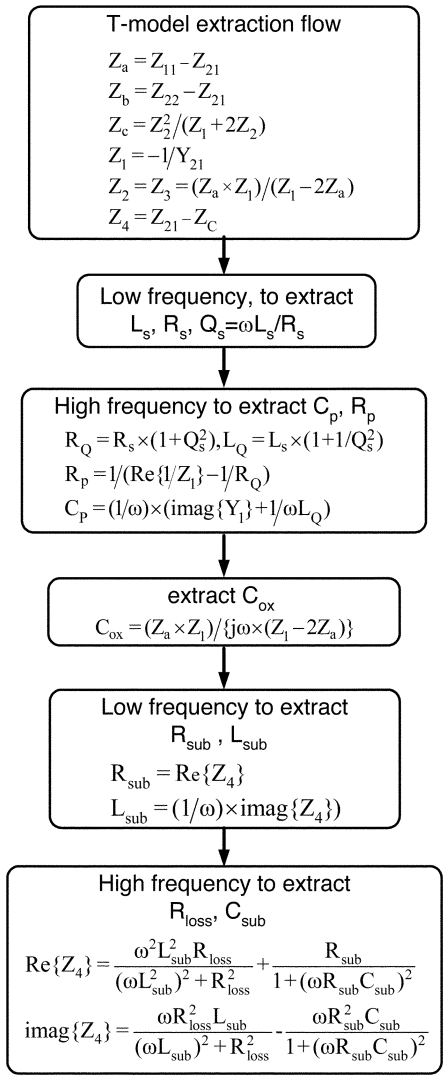

Fig. 2. T-model parameter formulas and extraction flow chart.

C. T-Model Parameter Extraction Flow and Physical Properties

As a result, all the physical elements composing the model can be extracted through the flow shown in Fig. 2. At the first step, R_S and L_S representing the physical inductor under very low frequency can be extracted. The ideal quality factor free from conductor and substrate losses, denoted as Q_S is given by $Q_S = \omega L_S/R_S$. After that, R_P and C_P can be extracted by close forms as a function of (R_S, L_S, Q_S) and measured $\mathrm{Y}_1(= 1/Z_1)$. C_P represents the inter-coil and underpass coupling capacitance, which is one of major elements to determine the frequency response, particularly the correct self-resonance frequency $(\omega_{\rm SR})$ and the phase near resonance. R_P is a new element introduced in our study to model the spiral conductor loss and Q degradation before resonance $(\omega < \omega_{\rm SR})$. Eddy current in the coil metal arising from the magnetic field generated through substrate return path under high frequency is proposed as the origin responsible for the additional spiral conductor loss represented by R_P [8]. $C_{\rm ox}$ is one more major element besides C_P to determine self-resonance frequency $(\omega_{\rm SR})$ and can be derived by the equation of Z-parameters shown in the flow chart.

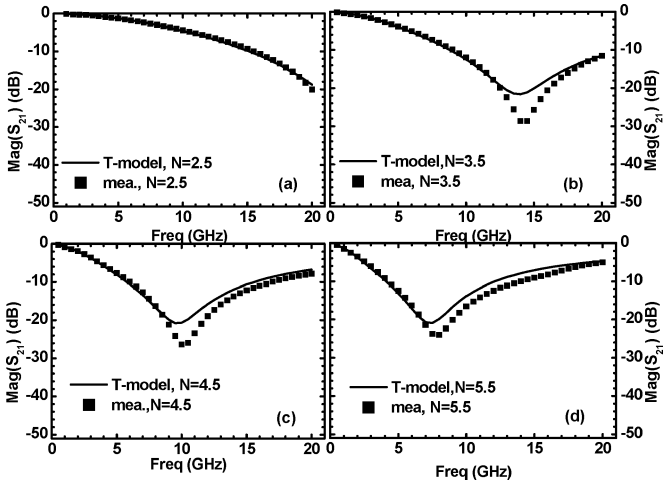

Fig. 3. Comparison of S_{21}(magnitude) between T-model simulation and measurement for spiral inductors. Coil numbers (a) $N = 2.5$, (b) $N = 3.5$, (c) $N = 4.5$, and (d) $N = 5.5$.

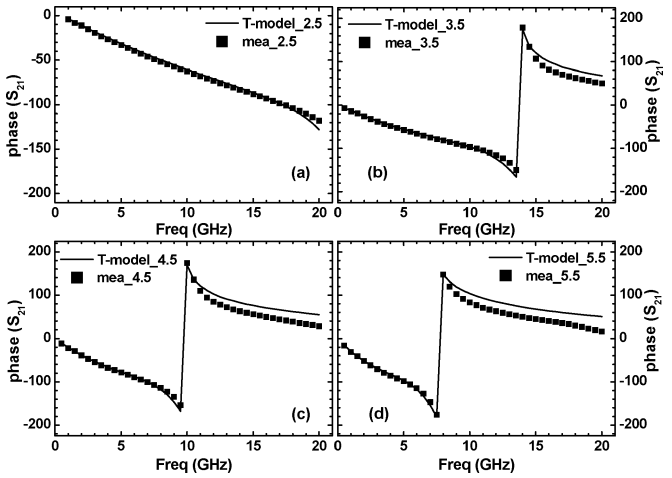

Fig. 4. Comparison of S_{21}(phase) between T-model simulation and measurement for spiral inductors. Coil numbers (a) $N = 2.5$, (b) $N = 3.5$, (c) $N = 4.5$, and (d) $N = 5.5$.

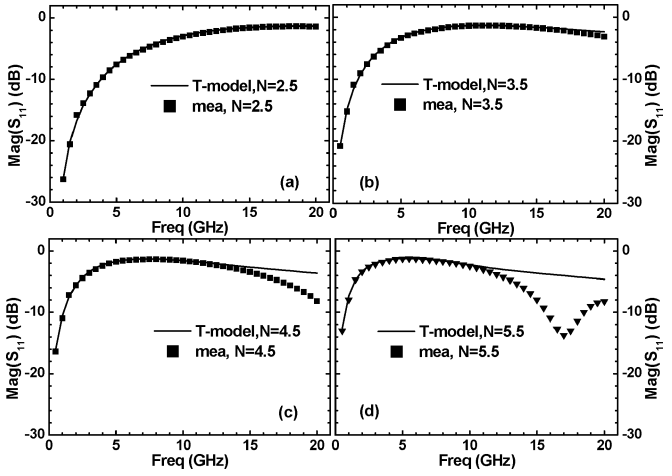

Fig. 5. Comparison of S_{11}(magnitude) between T-model simulation and measurement for spiral inductors. Coil numbers (a) $N = 2.5$, (b) $N = 3.5$, (c) $N = 4.5$, and (d) $N = 5.5$.

Then, $L_{\rm sub}$ and $R_{\rm sub}$ can be extracted easily from Z_4 under very low frequency provided that $R_{\rm loss}$ and $1/\omega C_{\rm sub}$ are relatively high impedances compared to $\omega L_{\rm sub}$ and $R_{\rm sub}$ and can be approximated as an open path. To the end, $C_{\rm sub}$ and $R_{\rm loss}$ can be extracted by the formulas shown in the last stage of flow chart based on all the known parameters and measured Z_4. $R_{\rm sub}$ is generally used to account for substrate resistance and the associated energy loss. $L_{\rm sub}$ is another new element introduced in our T-model to simulate the eddy current generated on the Si substrate, which is expected in opposite direction against the current flow in the spiral coils according to the Lenz' law. $L_{\rm sub}$ is required to accurately model frequency response of L and Re$(Z_{\rm in})$ near resonance but its effect on peak Q is negligible. On the other hand, $R_{\rm sub}$ has quite obvious effect on Q degradation over wide band. $L_{\rm sub}$, $R_{\rm sub}$, and R_P are required simultaneously to describe the substrate loss precisely in terms of $Q(\omega)$, $L(\omega)$, Re$(Z_{\rm in}(\omega))$, and phase angle at different frequencies. $C_{\rm sub}$ has been generally used in conventional π-model and it is justified as necessary for T-model to account for the degradation of $\omega_{\rm SR}$ and Q. $R_{\rm loss}$ is the last one in total 3 new elements (R_P, $L_{\rm sub}$, and $R_{\rm loss}$) introduced in our T-model. $R_{\rm loss}$ plays its role apparent near or beyond resonance. Lack of $R_{\rm loss}$ will leave $L_{\rm sub}$ alone and lead to abnormal double hump in S-parameters, $L(\omega)$, and Re$(Z_{\rm in}(\omega))$ beyond resonance.

IV. Broadband Accuracy and Scalability of Model

A. Broadband Accuracy

The proposed T-model has been extensively verified by comparison with measurement in terms of S-parameters (S_{11}, S_{21}), $L(\omega)$, Re$(Z_{\rm in}(\omega))$, and $Q(\omega)$ over broad bandwidth up to 20 GHz. The scalability is validated by various geometries with split of coil numbers, $N = 2.5$, 3.5, 4.5, and 5.5. Broadband accuracy is justified by good match with measurement in terms of the mentioned key performance parameters. Fig. 3(a)–(d) indicates the comparison for magnitude of S_{21} (Mag(S_{21})) between the T-model and measurement. Excellent match is achieved for all coil numbers before resonance and agreement of curvature is maintained beyond resonance, which happened at $f_{\rm SR} \ll$ 20 GHz ($f_{\rm SR} = \omega_{\rm SR}/2\pi$: self-resonance frequency) for larger coil numbers ($N = 4.5$ and 5.5). Fig. 4(a)–(d) shows the good agreement in terms of phase(S_{21}) in which precise match of resonance frequency $(f_{\rm SR})$ is demonstrated for all coil numbers. Fig. 5(a)–(d) reveals the exact match of Mag(S_{11}) for smaller coils ($N = 2.5$, 3.5) over full frequency range up to 20 GHz, which is well beyond resonance. Regarding the deviation beyond resonance for larger coils ($N = 4.5$, 5.5) with $f_{\rm SR} = 6.9$, 5.1 GHz, i.e., far below 20 GHz, it happened to be a common issue suffered by EM simulation and will deserve more study. Fortunately, this deviation did not make effect on the accuracy of $L(\omega)$, Re$(Z_{\rm in}(\omega))$, and $Q(\omega)$ beyond resonance. Again, Fig. 6(a)–(d) confirms the model accuracy in terms of phase(S_{11}) over broadband beyond resonance for each coil number.

More extensive verification has been done by comparison of four key performance parameters for spiral inductors, i.e., $L(\omega)$, Re$(Z_{\rm in}(\omega))$, $Q(\omega)$, and $\omega_{\rm SR}$. $L(\omega)$ is the imaginary part of input impedance $Z_{\rm in}(\omega)$, i.e., $\omega L(\omega) = {\rm Im}(Z_{\rm in}(\omega))$ while Re$(Z_{\rm in}(\omega))$ represents the real part of $Z_{\rm in}(\omega)$. $Q(\omega)$

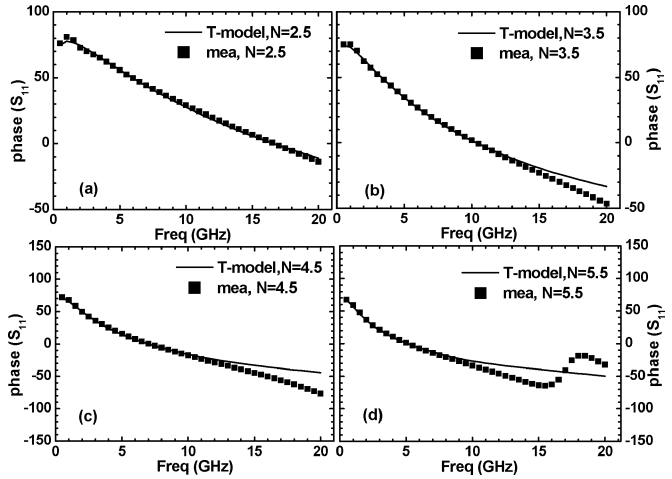

Fig. 6. Comparison of S_{11}(phase) between T-model simulation and measurement for spiral inductors. Coil numbers (a) $N = 2.5$, (b) $N = 3.5$, (c) $N = 4.5$, and (d) $N = 5.5$.

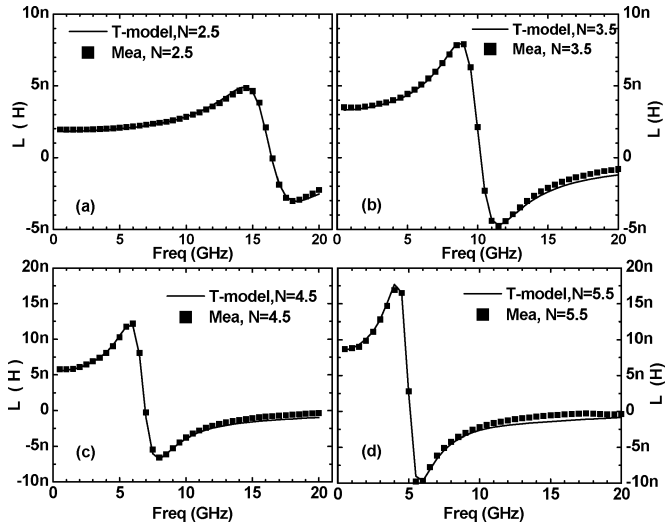

Fig. 7. Comparison of $L(\omega)$ between T-model simulation and measurement for spiral inductor with various coil numbers (a) $N = 2.5$, (b) $N = 3.5$, (c) $N = 4.5$, and (d) $N = 5.5$.

is the quality factor defined by $\omega L(\omega)/\mathrm{Re}(Z_{\mathrm{in}}(\omega)$. All three parameters are frequency dependent that is critically related to the spiral conductor loss and Si substrate loss. In fact, accurate simulation to predict $L(\omega)$, $\mathrm{Re}(Z_{\mathrm{in}}(\omega))$, and $Q(\omega)$ is the major goal of inductor models for circuit design and EM simulators for physical element design. In our study, the proposed T-model can provide very good match with the measurement for all the three parameters as follows. Fig. 7(a)–(d) illustrates the excellent fit to the measured $L(\omega)$ by our T-model for all spiral inductors operating up to 20 GHz. The transition from inductive to capacitive mode evoked by increasing frequency beyond f_{SR} is accurately reproduced by the model. Regarding $\mathrm{Re}(Z_{\mathrm{in}}(\omega))$, pretty good match between the T-model and measurement is shown in Fig. 8(a)–(d). The T-model can exactly capture the full band behavior of $\mathrm{Re}(Z_{\mathrm{in}}(\omega))$ even beyond resonance such as the dramatic increase prior to resonance, peak at resonance, and then sharp drop after the peak. Eventually, $Q(\omega)$ is of the primary concern for inductor design and the first key parameter governing RF IC performance such as power, gain, and noise

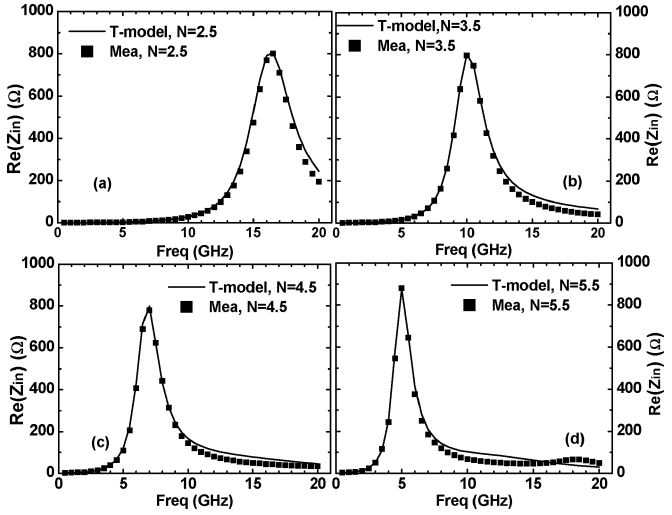

Fig. 8. Comparison of $\mathrm{Re}(Z_{\mathrm{in}}(\omega))$ between T-model simulation and measurement for spiral inductors with various coil numbers (a) $N = 2.5$, (b) $N = 3.5$, (c) $N = 4.5$, and (d) $N = 5.5$.

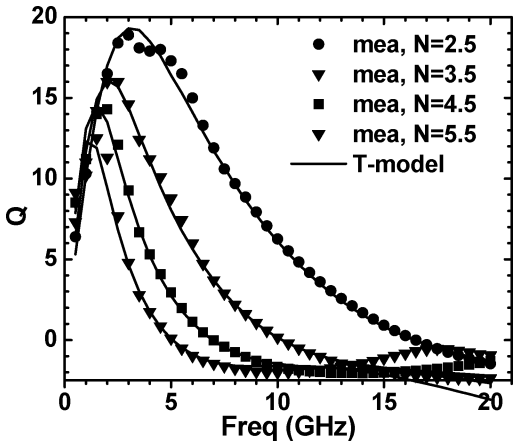

Fig. 9. Comparison of $Q(\omega)$ between T-model simulation and measurement for spiral inductor with various coil numbers: N =2.5, 3.5, 4.5, and 5.5.

figure, etc. Fig. 9 reveals the excellent match with the measured $Q(\omega)$ over the broad bandwidth of 20 GHz. The exact fit to the peak Q and capture of full band behavior for all coil numbers suggests the advantage of our T-model compared to the existing π-model. Self-resonance frequency f_{SR} is a key parameter accompanying with $Q(\omega)$ to quantify the useful bandwidth. In our T-model, f_{SR} can be accurately predicted by both full equivalent circuit simulation and analytical model of closed form given by (1). The analytical model is readily derived by equivalent circuit analysis on this new T-model and a simple formulas by closed form expressed as (1) is derived under appropriate approximation. The details of model equation derivation can be referred to the Appendix. The approximation made by removing L_{sub} and R_{loss} was justified by impedance analysis and equivalent circuit simulation. Fig. 10 presents $Q(\omega)$ calculated by reduced T-model without L_{sub} and R_{loss} and the comparison with original T-model with L_{sub} and R_{loss}.The major difference is revealed in higher frequency region beyond the peak Q but the intercept point corresponding to $Q = 0$, i.e., f_{SR} is nearly identical to each other. Table I lists the exact values of f_{SR} for comparison among measurement,

TABLE I
COMPARISON OF SELF-RESONANCE FREQUENCY ($f_{\rm SR}$) AMONG MEASUREMENT, SIMULATION BY ORIGINAL T-MODEL AND REDUCED T-MODEL, AND CALCULATION BY ANALYTICAL MODEL

N	f_{SR}, Measured (GHz)	f_{SR}, Original T-model (GHz)	f_{SR}, Reduced T-model L_{sub}=0, R_{loss}=0 (GHz)	f_{SR}, Analytical model L_{sub}=0, R_{loss}=0 (GHz)	f_{SR}, T-model simulation L_{sub}=0, R_{loss}=0
2.5	16.4	16.43	16.402	16.474	17.15
3.5	10.2	10.214	10.258	10.362	10.92
4.5	6.9	6.944	6.975	7.18	7.64
5.5	5.1	5.071	5.16	5.326	5.73

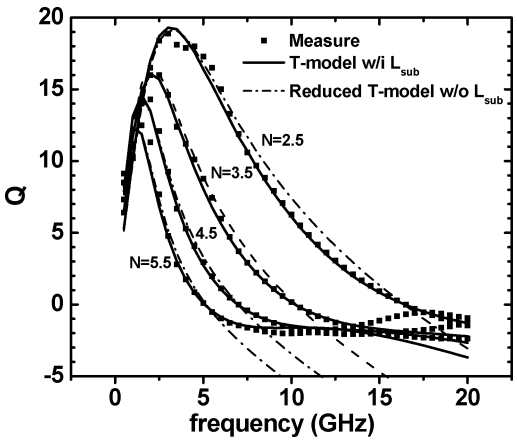

Fig. 10. Comparison of $Q(\omega)$ and self-resonance frequency $f_{\rm SR}$ corresponding to $Q = 0$ among T-model, reduced T-model ($L_{\rm sub} = R_{\rm loss} = 0$) and measurement for spiral inductors with various coil numbers.

simulation by original T-model and reduced T-model, and calculation by analytical model of (1). The good agreement to each other in terms of deviation below 0.2 GHz justifies the approximation for reduced T-model and the derived analytical model for $f_{\rm SR}$. The accuracy of $f_{\rm SR}$ calculated by the equivalent circuit simulation and analytical model is further validated by good match with the measured results shown in Fig. 11(a) for various coil numbers. Regarding the parasitic capacitance effect on $f_{\rm SR}$ as mentioned previously, Fig. 11(b) indicates the C_P, $C_{\rm ox}$, and $C_{\rm sub}$ effect on $f_{\rm SR}$ predicted by ADS simulation using full equivalent circuit and analytical model given by (1). The results from ADS simulation and analytical model show very good consistency. We see that the elimination of C_P or $C_{\rm sub}$ can help to increase $f_{\rm SR}$ by around 15∼20% corresponding to $N = 2.5$, 3.5, 4.5, 5.5 while the elimination of $C_{\rm ox}$ can dramatically boost $f_{\rm SR}$ by more than 100%, i.e., more than double the existing performance for all coil numbers. The prediction from our T-model suggests that $C_{\rm ox}$ plays a dominant role in determining $f_{\rm SR}$ and spiral inductor on package is a potential solution to minimize $C_{\rm ox}$ and achieve maximum $f_{\rm SR}$. Recently, low temperature co-fire ceramic (LTCC) has been promoted as a useful process to implement the RF passive elements on package wherein effective enhancement of Q and $f_{\rm SR}$ has been demonstrated [9], [10]

$$f_{\rm SR} = \frac{1}{2\pi}\sqrt{\frac{1}{L_s}\times\left(\frac{C_{\rm ox1}+C_{\rm ox2}+C_{\rm sub}}{C_p(C_{\rm ox1}+C_{\rm ox2}+C_{\rm sub})+C_{\rm ox1}(C_{\rm sub}+C_{\rm ox2})}\right)} \quad (1)$$

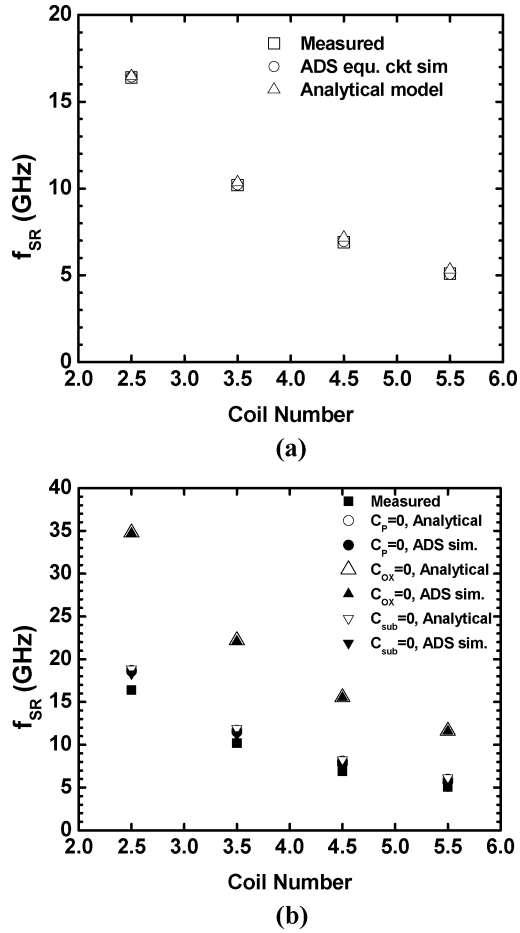

Fig. 11. Self-resonance frequency $f_{\rm SR}$ of on-chip spiral inductors with various coil numbers, $N = 2.5$, 3.5, 4.5, 5.5 (a) comparison between measurement, ADS simulation, and analytical model (b) C_P, $C_{\rm ox}$, and $C_{\rm sub}$ effect on $f_{\rm SR}$ calculated by ADS simulation and analytical model. Comparison with measured $f_{\rm SR}$ to indicate the $f_{\rm SR}$ increase contributed by eliminating the parasitic capacitances, C_P, $C_{\rm ox}$, and $C_{\rm sub}$ respectively.

B. Skin Effect–Frequency Dependent R_S in Conventional Model and Constant R_P in T-Model for Broadband Accuracy

Regarding the skin and current crowding effects, which are considered playing an important role on Q, a frequency dependent R_S is generally proposed to fit the frequency response of Q over wide band. Through our study, the frequency dependent R_S, i.e., $R_S(\omega)$ formulated by the ideal model given by (2) is adopted and implemented to our T-model in which R_P was removed to manifest $R_S(\omega)$ effect alone. The simulated $Q(\omega)$ shown in Fig. 12 reveals obvious deviation from measured one over frequencies beyond that of peak Q and suggests that $R_S(\omega)$ alone cannot simulate the frequency response accurately even

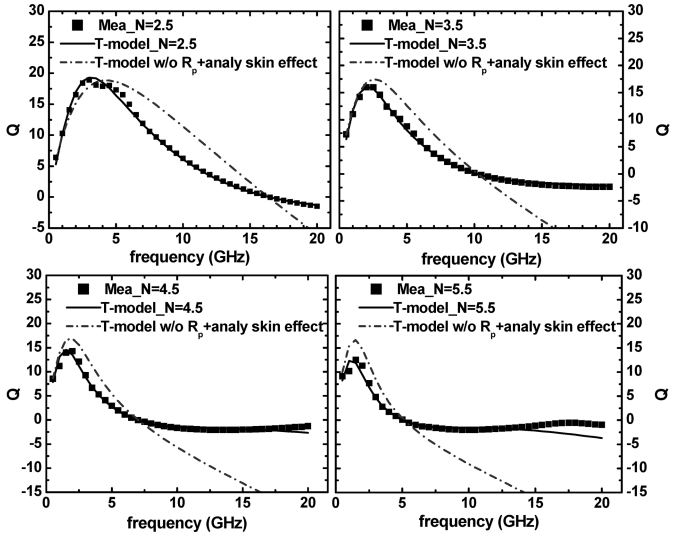

Fig. 12. $Q(\omega)$ calculated by equivalent circuit removing R_P from original T-model and adding $R_S(\omega)$ to simulate skin effect for spiral inductors with various coil numbers (a) $N = 2.5$, (b) $N = 3.5$, (c) $N = 4.5$, and (d) $N = 5.5$.

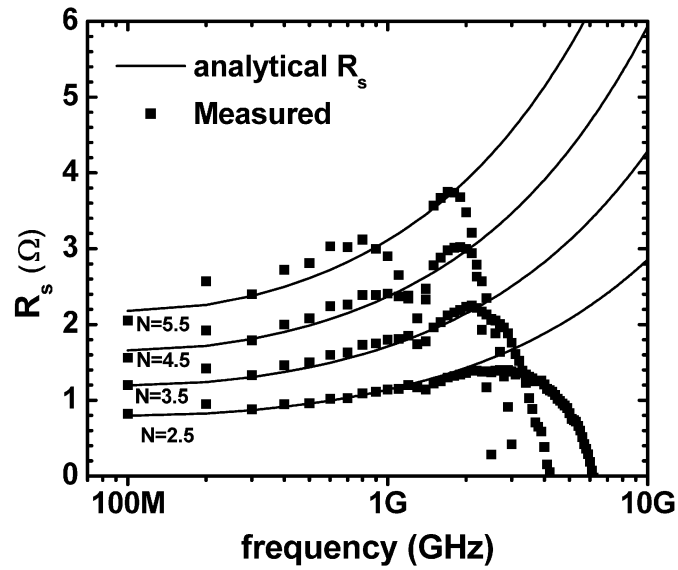

Fig. 13. Frequency dependent R_S extracted from measurement through definition of $R_S(\omega) = \mathrm{Re}(-/Y_{21})$ and the comparison with $R_S(\omega)$ calculated by ideal model of (2) for spiral inductors with various coil numbers, N =2.5, 3.5, 4.5, and 5.5.

in narrow band around the peak Q. Besides, the frequency dependent elements are generally difficult to be implemented in time-domain simulators such as SPICE [11]. To verify the origin responsible for the deviation, $R_S(\omega)$ calculated by ideal model (2) is compared with the measured $R_S = \mathrm{Re}(-1/Y_{21})$. The result shown in Fig. 13 indicates that the ideal model can accurately fit R_S at very low frequencies ($f < 2$ GHz) but over-estimates R_S at frequencies beyond 2 GHz for all inductors of different coil numbers. The roll-off of $R_S(\omega)$ revealed at higher frequency is proposed to stem from lateral substrate coupling effect [6]. It is very interesting to note that the dramatic increase of $R_S(\omega)$ predicted by skin-effect model at higher frequency is actually an over-estimation compared to the measured one but cannot help to accurately reproduce Q degradation at frequencies near or beyond the peak Q. In our T-model, R_P has been

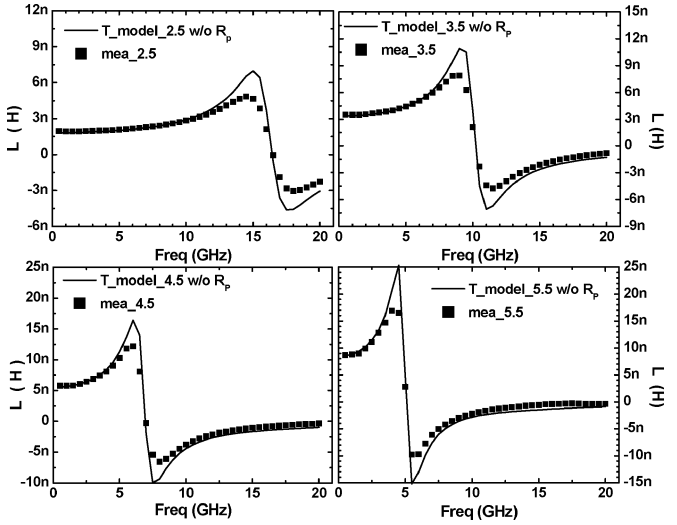

Fig. 14. $L(\omega)$ calculated by equivalent circuit simulation with R_P removed from original T-model for spiral inductors with various coil numbers (a) $N = 2.5$, (b) $N = 3.5$, (c) $N = 4.5$, and (d) $N = 5.5$.

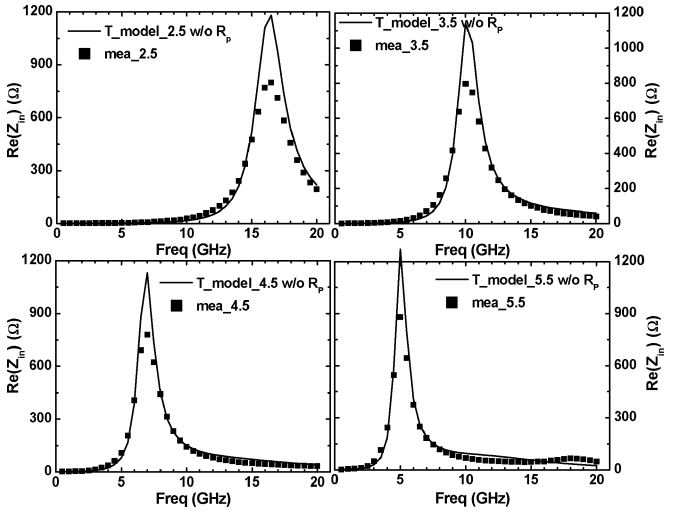

Fig. 15. $\mathrm{Re}(Z_{\mathrm{in}}(\omega))$ calculated by equivalent circuit simulation with R_P removed from original T-model for spiral inductors with various coil numbers (a) $N = 2.5$, (b) $N = 3.5$, (c) $N = 4.5$, and (d) $N = 5.5$.

introduced as a new element to account for the spiral conductor loss and Q degradation over wide band. To justify the role played by R_P, simulation was done by removing R_P from the original T-model to verify the impact on $L(\omega)$, $\mathrm{Re}(Z_{\mathrm{in}}(\omega))$, and $Q(\omega)$ as shown in Figs. 14, 15, and 16 respectively. We see that R_P in this model has obvious effect on $L(\omega)$ and $\mathrm{Re}(Z_{\mathrm{in}}(\omega))$ at high frequency near resonance and significant impact on Q over wide band The physical property and origin as defined previously for R_P, i.e., eddy current in the coil metal arising from the magnetic field generated through substrate return path is believed an appropriate mechanism to account for the broadband characteristics in terms of $L(\omega)$, $\mathrm{Re}(Z_{\mathrm{in}}(\omega))$, and $Q(\omega)$ as demonstrated

$$R_S(\omega) = \frac{L}{W \cdot \sigma \cdot \delta(\omega) \cdot \left(1 - e^{\frac{-t}{\delta}}\right)}$$
$$\delta(\omega) = \left(\frac{1}{\omega\mu\sigma}\right)^{\frac{1}{2}} \quad (2)$$

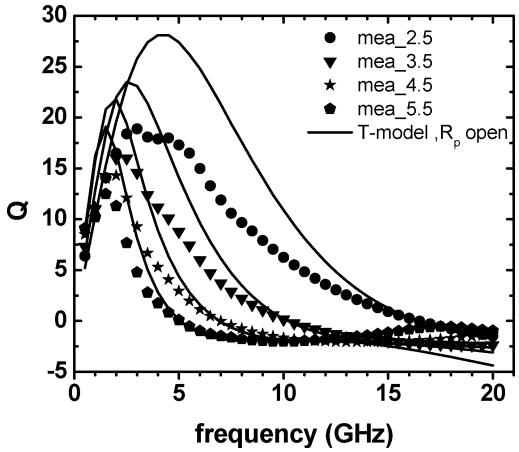

Fig. 16. $Q(\omega)$ calculated by equivalent circuit simulation with R_P removed from original T-model for spiral inductors with various coil numbers (a) $N = 2.5$, (b) $N = 3.5$, (c) $N = 4.5$, and (d) $N = 5.5$.

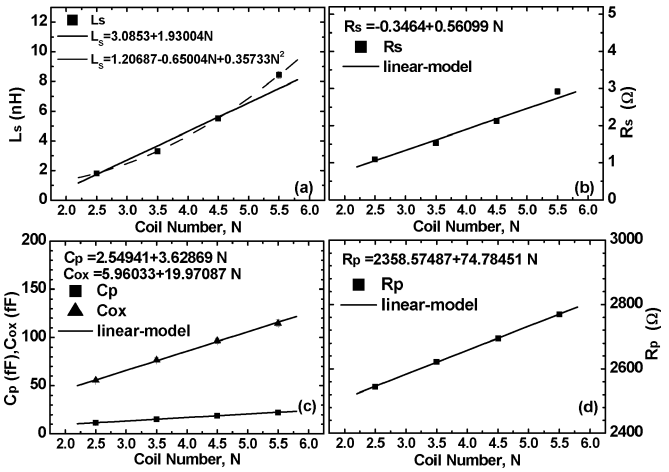

Fig. 17. T-model RLC network parameters versus coil numbers, spiral coil's RLC network parameters (a) L_S, (b) R_S, (c) C_P and $C_{\rm ox}$, and (d) R_P.

where *L,W,* and *t* are the metal line length, width, and thickness, respectively. σ is the conductivity, μ is the permeability, and $\delta(\omega)$ represents the skin depth of frequency dependence.

C. Model Scalability

Besides the broadband accuracy as presented, another important feature realized by this T-model is the good scalability w.r.t. geometry for all model parameters. Fig. 17 reveals good match with a linear function of coil numbers for each model parameter in the spiral coil's *RLC* network, i.e., R_S, L_S, R_P, C_P, and $C_{\rm ox}$. All five elements present monotonically increasing function of coil number in which coefficient of first order derivative has been extracted for every parameter. In reality, the inductance *L* follows a curve more complicated than linear function. As shown in Fig. 17(a), *L* can be precisely fitted by a parabolic function of *N* (coil number). Fig. 18 indicates the excellent fit by linear function for substrate *RLC* network involved model parameters, $1/R_{\rm sub}$, $C_{\rm sub}$, $L_{\rm sub}$, and $R_{\rm loss}$. The decrease of $R_{\rm sub}$ or increase of $1/R_{\rm sub}$ corresponding to larger coil number accounts for the worse substrate loss caused by increasing spiral coil size. Regarding $C_{\rm sub}$, $L_{\rm sub}$, and $R_{\rm loss}$, all three terms follow linearly increasing function of *N*. The scaling behavior revealed by the four parameters is physically derivable and sufficiently

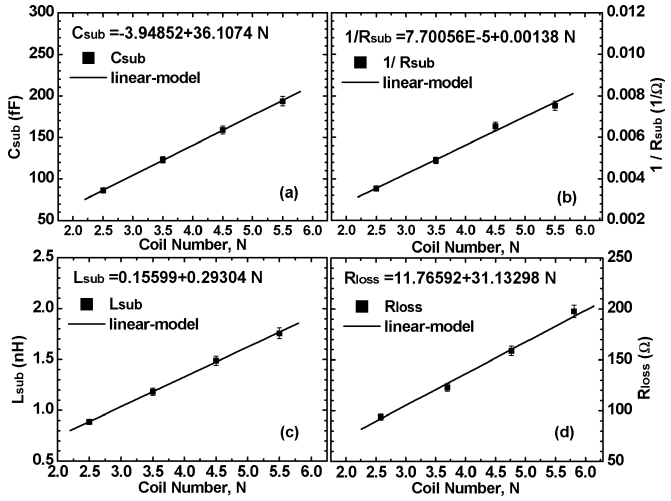

Fig. 18. T-model RLC network parameters versus coil number, lossy substrate RLC network parameters (a) $C_{\rm sub}$, (b) $1/R_{\rm sub}$, (c) $L_{\rm sub}$, and (d) $R_{\rm loss}$.

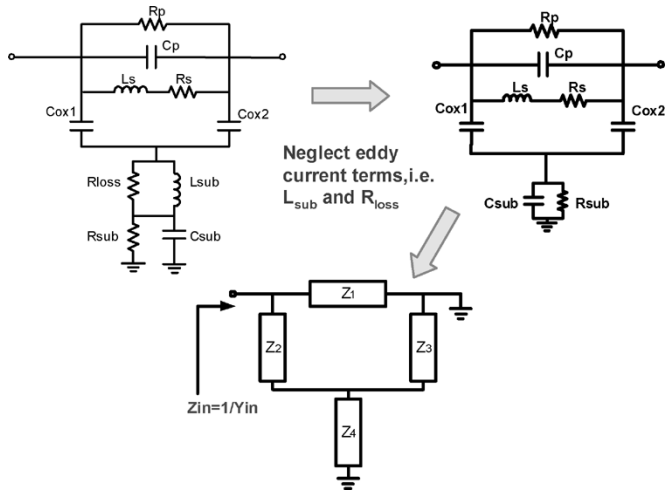

Fig. 19. Equivalent circuit schematics and analysis of reduce T-model to derive the analytical model for calculating self-resonance frequency $f_{\rm SR}$

accurate to calculate substrate loss effect on $L(\omega)$, $Q(\omega)$, and $f_{\rm SR}$, etc. for inductor of various spiral coil sizes. Regarding interest in more extensive scope of layout geometries such as coil metal width or inner radius, a preliminary work has been done to validate the model over wide range of widths (3, 9, 15, and 30 μm). Good fit to all measured parameters as mentioned can be maintained and model scalability is presented as a parabolic function instead of a linear function. A minor modification to the original T-model by adding an inductor element (L_P) in series with R_P to account for proximity effect can further improve the fitting accuracy. The detail will not be covered by this paper due to limited pages. The promisingly good scalability proven for full set of model parameters as demonstrated suggests that this T-model is useful in pre-layout simulation and optimization for physical design. The nature of easy link with standard circuit simulator makes this T-model useful in circuit element tuning and optimization for RF circuit design.

V. Conclusion

A broadband and scalable T-model has been developed to accurately simulate on-chip spiral inductors operating up to 20 GHz.

under the approximation (A7), (A8), (A9)

$$\omega C_p - \frac{1}{R_s^2}\frac{\omega L_s}{1+\left(\frac{\omega L_s}{R_s}\right)^2} + \frac{\omega C_{\rm ox1} + \omega^3 R_{\rm sub}^2 C_{\rm ox1} C_T (C_{\rm sub}+C_{\rm ox2})}{1+(\omega R_{\rm sub} C_T)^2} = 0$$

$$\Rightarrow \omega^2 \left(\frac{C_{\rm ox1}(C_{\rm sub}+C_{\rm ox2})}{C_T} + C_p\right)\Bigg|_{\omega=\omega_{\rm SR}} = \frac{1}{L_s} \tag{A10}$$

$$\Rightarrow \omega_{\rm SR} = \sqrt{\frac{1}{L_s} \times \left(\frac{C_{\rm ox1}+C_{\rm ox2}+C_{\rm sub}}{C_p(C_{\rm ox1}+C_{\rm ox2}+C_{\rm sub}) + C_{\rm ox1}(C_{\rm sub}+C_{\rm ox2})}\right)} \tag{A11}$$

$$\therefore f_{\rm SR} = \frac{1}{2\pi}\sqrt{\frac{1}{L_s} * \left(\frac{C_{\rm ox1}+C_{\rm ox2}+C_{\rm sub}}{C_p(C_{\rm ox1}+C_{\rm ox2}+C_{\rm sub}) + C_{\rm ox1}(C_{\rm sub}+C_{\rm ox2})}\right)} \tag{A12}$$

A parameter extraction flow has been established through equivalent circuit analysis to enable automatic parameter extraction and optimization. Good scalability is validated for all model parameters and manifests the physical property underlying each parameter. The results suggest that the proposed T-model can facilitate Si CMOS based RF IC design adopting on-chip inductors.

APPENDIX

The analytical model equation for calculating self-resonance frequency, $f_{\rm SR}$ is derived based on reduced T-model equivalent circuit analysis as shown in Fig. 19 and mathematical formulas development as follows:

$$\begin{aligned} Y_{\rm in} &= \frac{1}{Z_1} + \frac{1}{Z_2 + \frac{Z_3 * Z_4}{Z_3+Z_4}} \\ &= \frac{1}{R_p} + sC_p + \frac{1}{R_s+sL_s} + \frac{1}{\frac{1}{sC_{\rm ox1}} + \frac{R_{\rm sub}}{1+sR_{\rm sub}(C_{\rm sub}+C_{\rm ox2})}} \\ &= \frac{1}{R_p} + sC_p + \frac{1}{R_s+sL_s} \\ &\quad + \frac{sC_{\rm ox1} - s^2 R_{\rm sub} C_{\rm ox1}(C_{\rm sub}+C_{\rm ox2})}{1+sR_{\rm sub}(C_{\rm ox1}+C_{\rm ox2}+C_{\rm sub})} \end{aligned} \tag{A1}$$

$$\begin{aligned} s &= j\omega \\ C_T &= C_{\rm ox1}+C_{\rm ox2}+C_{\rm sub} \end{aligned} \tag{A2}$$

$$\begin{aligned} Y_{\rm in} &= \frac{1}{R_p} + j\omega C_p + \frac{1}{R_s}\frac{1}{1+\left(\frac{\omega L_s}{R_s}\right)^2} \\ &\quad - j\frac{1}{R_s^2}\frac{\omega L_s}{1+\left(\frac{\omega L_s}{R_s}\right)^2} + \frac{\omega^2 R_{\rm sub} C_{\rm ox1}^2}{1+(\omega R_{\rm sub} C_T)^2} \\ &\quad + j\frac{\omega C_{\rm ox1} + \omega^3 R_{\rm sub}^2 C_{\rm ox1} C_T (C_{\rm sub}+C_{\rm ox2})}{1+(\omega R_{\rm sub} C_T)^2} \end{aligned} \tag{A3}$$

$$\begin{aligned} Q &= \frac{Im\left(\frac{1}{Y_{\rm in}}\right)}{{\rm Re}\left(\frac{1}{Y_{\rm in}}\right)} \\ &= \frac{\omega C_p - \frac{1}{R_s^2}\frac{\omega L_s}{1+\left(\frac{\omega L_s}{R_s}\right)^2} + \frac{\omega C_{\rm ox1} + \omega^3 R_{\rm sub}^2 C_{\rm ox1} C_T (C_{\rm sub}+C_{\rm ox2})}{1+(\omega R_{\rm sub} C_T)^2}}{\frac{1}{R_p} + \frac{1}{R_s}\frac{1}{1+\left(\frac{\omega L_s}{R_s}\right)^2} + \frac{\omega^2 R_{\rm sub} C_{\rm ox1}^2}{1+(\omega R_{\rm sub} C_T)^2}} \end{aligned} \tag{A4}$$

$$Q(\omega=\omega_{\rm SR}) = 0 \Rightarrow {\rm Im}\left(\frac{1}{Y_{\rm in}(\omega)}\right)\Bigg|_{\omega=\omega_{\rm SR}} = 0 \tag{A5}$$

$$\begin{aligned} &\omega C_p - \frac{1}{R_s^2}\frac{\omega L_s}{1+\left(\frac{\omega L_s}{R_s}\right)^2} \\ &\quad + \frac{\omega C_{\rm ox1}\left[1+\omega^2 R_{\rm sub}^2 C_T (C_{\rm sub}+C_{\rm ox2})\right]}{1+(\omega R_{\rm sub} C_T)^2}\Bigg|_{\omega=\omega_{\rm SR}} = 0 \end{aligned} \tag{A6}$$

$$\begin{aligned} &C_T = C_{\rm ox1}+C_{\rm ox2}+C_{\rm sub} \\ &\omega \to \omega_{\rm SR} : (\omega R_{\rm sub} C_T)^2 \gg 1 \\ &\quad \to 1+(\omega R_{\rm sub} C_T)^2 \approx (\omega R_{\rm sub} C_T)^2 \end{aligned} \tag{A7}$$

$$\begin{aligned} &\omega \to \omega_{\rm SR} : \omega^2 R_{\rm sub}^2 C_T (C_{\rm sub}+C_{\rm ox2}) \gg 1 \\ &\quad \therefore 1+\omega_2 R_{\rm sub}^2 C_T (C_{\rm sub}+C_{\rm ox2}) \\ &\quad \approx \omega^2 R_{\rm sub}^2 C_T (C_{\rm sub}+C_{\rm ox2}) \end{aligned} \tag{A8}$$

$$\begin{aligned} &\omega \to \omega_{\rm SR} : \left(\frac{\omega L_s}{R_s}\right)^2 \gg 1 \\ &\quad \to 1+\left(\frac{\omega L_s}{R_s}\right)^2 \approx \left(\frac{\omega L_s}{R_s}\right)^2 \end{aligned} \tag{A9}$$

ACKNOWLEDGMENT

The authors would like to thank the Chip Implementation Center for ECAD tool support.

REFERENCES

[1] C. P. Yue and S. S. Wong, "Physical modeling of spiral inductors on silicon," *IEEE Trans. Electron Devices*, vol. 47, no. 4, pp. 560–568, Apr. 2000.

[2] M. Park, S. Lee, C. S. Kim, H. K. Yu, and K. S. Nam, "The detailed analysis of high Q CMOS-compatible microwave spiral inductors in silicon technology," *IEEE Trans. Electron Devices*, vol. 45, no. 10, pp. 1953–1959, Oct. 1998.

[3] P. Arcioni, R. Castello, G. D. Astis, E. Sacchi, and F. S. Svelto, "Measurement and modeling of Si integrated inductors," *IEEE Trans. Instrum. Meas.*, vol. 47, no. 11, pp. 1372–1378, Nov. 1998.

[4] Y. Cao, R. A. Grove, X. Huang, N. D. Zamdmer, J.-O. Plouchart, R. A. Wachnik, T.-J. King, and C. Hu, "Frequency-independent equivalent-circuit model for on-chip spiral inductors," *IEEE J. Solid-State Circuits*, vol. 38, no. 5, pp. 419–426, May 2003.

[5] M. Fujishima and J. Kino, "Accurate subcircuit model of an on-chip inductor with a new substrate network," in *VLSI Symp. Tech. Dig.*, 2004, pp. 376–379.

[6] J. Gil and H. Shin, "A simple wide-band on-chip inductor model for silicon-based RF Ics," *IEEE Trans. Microw. Theory Techn.*, vol. 51, no. 12, pp. 2023–2028, Dec. 2003.

[7] T. S. Horng, J. K. Jau, C. H. Huang, and F. Y. Han, "Synthesis of a super broadband model for on-chip spiral inductors," in *IEEE RFIC Symp. Dig.*, 2004, pp. 453–456.
[8] A. M. Niknejad and R. G. Meyer, "Analysis of eddy-current losses over conductive substrate with applications to monolithic inductors and transformers," *IEEE Trans. Microw. Theory Techn.*, vol. 49, no. 1, pp. 166–176, Jan. 2001.
[9] A. Sutono, D. Heo, Y.-J. E. Chen, and J. Laskar, "High-Q LTCC-based passive library for wireless system-on-package (SOP) module development," *IEEE Trans. Microw. Theory Techn.*, vol. 49, no. 10, pp. 1715–1724, Oct. 2001.
[10] A. Sutono, D. Heo, E. Chen, K. Lim, and J. Laskar, "Compact implementation of component library in LTCC technology and its application to CMOS RF power amplifier design," in *Proc. IEEE Conf. Electr. Perf. Electron. Packag.*, Oct. 23–25, 2000, pp. 288–291.
[11] T. Kamgaing, T. Myers, M. Petras, and M. Miller, "Modeling of frequency dependent losses in two-port and three-port inductors on silicon," in *IEEE MTT-S Int. Microw. Symp. Dig.*, 2002, pp. 153–156.

Jyh-Chyurn Guo received the B.S.E.E. and M.S.E.E. degrees from National Tsing-Hua University (NTHU), Taiwan, R.O.C., in 1982 and 1984, respectively, and the Ph.D. degree in electronics engineering from the National Chiao-Tung University (NCTU), Hsinchu, Taiwan, in 1994.

Previously, she was working in the semiconductor industry with a focus on device design and VLSI technology development. In 1984, she joined the ERSO/ITRI, where she was engaged in semiconductor integrated circuit technologies with a broad scope to cover the high-voltage, high-power, submicron project, and high-speed SRAM technologies, etc. From 1994 to 1998, she was with Macronix International Corporation, where she was engaged in high-density and low-power flash memory technology development. In 1998, she joined Vanguard International Semiconductor Corporation, where she served as a Department Manager, responsible for advanced DRAM device technology development. In 2000, she joined Taiwan Semiconductor Manufacturing Company (TSMC), Hsinchu, where she served as a Program Manager in charge of 0.1-μm logic CMOS FEOL, high-performance-analog and RF CMOS technology development. She joined NCTU in 2003 as an Associate Professor in the Department of Electronics Engineering. Her current research interests cover RF CMOS and high-performance analog device design and modeling, novel nonvolatile memory technology, and circuit technology for SOC. She has authored or co-authored more than 40 technical papers and has been granted 12 international patents in her professional field.

Teng-Yang Tan was born in Taichung, Taiwan, R.O.C., in 1981. He received the B.S. degree in E.E. from National Taiwan University of Science and Technology, Taipei, Taiwan, R.O.C., in 2003. He is currently pursuing the M.S. degree at the Institute of Electronics, National Chiao-Tung University, Hsinchu, Taiwan, R.O.C.

His current research interests focus on RF passive device modeling and characterization.